Indian Journal of Chemical Technology
Vol. 30, May 2023, pp. 278-292
DOI: 10.56042/ijct.v30i3.69961

Spectral characterizations, Hirshfeld surface analysis and molecular docking studies of new novel NLO 2-(3,4-Dimethoxyphenyl)-3-hydroxy-4H-chromen-4-one

K Parimala
PG & Research Department of Physics, Nehru Memorial College, Trichy 621 007, Tamil Nadu, India
E-mail: kparimala79@yahoo.co.in

Received 27 December 2022; accepted 6 April 2023

The molecular structure of the compound, spectroscopic investigations (FT-IR, FT-Raman, and NMR) and the frontier energy level analysis of 2-(3,4-Dimethoxyphenyl)-3-hydroxy-4H-chromen-4-one (DMP3H), have been all examined using density functional theory (DFT) methods. Comparisons are made between predicted DFT geometrical parameters and experimental values and also the same performed between the theoretical vibrational wavenumbers and observed data. Chemical reactivity of DMP3H has been studied using DFT/PBEPBE approach that includes frontier orbital energies, optical characteristics and chemical descriptors. Additionally, the cytotoxic activity of the bioactive ligand has been checked against human cancer cell lines A549 and MCF-7 in vitro by the MTT assay. Hence, the docking and *in vitro* activity against cancer cell lines display positive results and the present ligand performance appears to be a promising way for anticancer agents with better efficacy.

Keywords: DFT, FT-IR, FT-Raman, MTT, NMR, PBEPBE

Cancer is one of the most significant human health issues worldwide and is among the leading causes of death. The four most frequently diagnosed cancers in men and women in 2021 were cancers of the lung, colorectal, breast, and bronchus, accounting for 45–52% of the total cancer cases in this group. One million new instances of cancer are expected to be identified each year in the US, and 608, 570 people will die from heart flu each year by 2021[1,2]. The toxicity associated with the traditional or standard anticancer therapy arises primarily from the lack of tumor specificity.

It leads to a narrow therapeutic index (NTI), which results in undesirable health effects to healthy tissues and consequently puts limitations on the dose of the medication that may be administered. Most majority of the presently to be had anticancer drugs are newly determined to have a highly selective toxicity toward different tumor cells[3-5]. Thus, pharmacological and phytochemical constituents have become the dignified group of effective antineoplastic against most of the cancer types. Over 50% of the available anticancer drugs FDA (Food and drug administration) approved from 1940 to 2014 were either natural products or directly derived therefrom. Therefore, the search for new promising small molecules for anticancer agents continues to draw attention to the scientific and research community in modern medicinal Chemistry.

Flavones is the nickname of 2-(3,4-Dimethoxyphenyl)-3-hydroxy-4H-chromen-4-one (DMP3H), which belongs to biologically active flavonoid-based compounds universally found in the plant kingdom[6]. The flavonoids are a family of polyphenolic compounds play much of significant role in defense system against insects, DNA (Deoxyribonucleic acid) microorganisms, and ultraviolet radiation or aggression by pathogens[7, 8]. The strongest evidence from in vitro studies has recommended that flavone derivatives are also health-beneficial to human and cell cultures or animal models. Because of their most abundant for many foods including fruits, herbs, vegetables and medicinal plants[9], flavones are common nutrients that are antibacterial, antiviral, anticancer, anti-inflammatory, cytotoxicity and estrogenic agents[10-13]. It has been seen that flavones may be possibility of developing prevention of cancer cells. The pharmacological effects of flavones may block cancer cells through several stages in the progression of carcinogenicity such as cell transformation, survival, proliferation, angiogenesis or active suppression, migration, activating invasion and metastasis, through cyclin-dependent kinases (CSKs), regulating cell

cycle, reducing transcription factors and also apoptotic cell death.

The luteolin is most commonly present in a bunch of rich foods, fruits and vegetables including parsley, leaves (spinach, lettuce and onion), stalk (celery), carrots, peppers, cabbages, apple skins, and chrysanthemum flowers. Pharmacological applications of flavone compounds are limited by poor water solubility or low permeability, poor aqueous solubility and low bioavailability. Belonging to the flavone group of flavonoids, luteolin has been modified by the structure, functionalization of two aromatic benzene (A and B) rings and structural manipulation of the methyl groups. Currently, the cell viability, migration and invasion studies have focused on discovering new luteolin anticancer drugs in terms of specific target, particularly from the natural, hemisynthetic and synthetic products have been identified as remarkable small molecule agents with effective application[14, 15].

The focus of the present research, we have performed experimental and computational studies on luteolins based metheoxy group substituted 2-(3,4-Dimethoxyphenyl)-3-hydroxy-4H-chromen-4-one (DMP3H) compound. The comprehensive study on optimized molecular geometry, Hirshfeld surface, spectroscopic properties and the bioactive compound has also been biologically studied for potent in vitro cytotoxic activity, studying the MTT assay against human cancer cell lines and along with the docking analysis. According to our research, no one has conducted a thorough theoretical investigation of optimum molecular geometries and spectroscopic examination of this chemical. Hirshfeld surface calculations examine the molecular surface analysis of intermolecular hydrogen bonding interactions. Chemical descriptors, optical properties, and computational analysis of intramolecular electron transport and atomic charge transfer have all been explored utilizing this level of technique, the PBEPBE/6-311++G(d,p). Additionally, molecular docking research is used to examine the title molecule's interaction residues and binding free energy in order to determine whether or not they might serve as target protein inhibitors. Using an MTT test, the medicinal molecule's cell viability was confirmed to have cytotoxic action against human cancer cell lines.

Experimental Section

Compounds of the 2-(3,4-Dimethoxyphenyl)-3-hydroxy-4H-chromen-4-one (DMP3H) ($C_{17}H_{14}O_5$) was analyzed using the usual KBr pallet technique in the 4000–400 cm^{-1} range on a TENSOR 27 type spectrometer with a 2 cm^{-1} resolution. Bruker IFS 66 V optical bench and FRA 106 Raman module were used in conjunction with a Nd:YAG laser and wavenumber mode of a FRA 106 Raman module to obtain 4000–50 cm^{-1} wavelength Raman spectra. The proton nuclear magnetic resonance (NMR) spectrum was carried out on a Bruker model AMX 500 spectrometer, using deuterated chloroform solvent with internal standard TMS.

Biological studies-cell culture and reagents

Sigma Aldrich Chemicals Pvt. Ltd. provided the streptomycin, penicillin, streptomycin-glutamine, ethanol, DMSO and EDTA used in the study. Dulbecco's Modified Eagle Medium (DMEM) was the first medium provided by Sigma Aldrich Chemicals Pvt. Ltd. (India). It was acquired from NCCS, Pune, the human cancer cell lines (A549 and MCF-7) Mosmann's MTT test was used to assess the cell viability of title compound on lung and breast cancer cells. Reduction of a yellow tetrazolium salt was used to conduct the cytotoxicity investigation on A549 and MCF-7 cell lines (MTT). The enzyme, NADH-cytochrome P-450 reductase, is involved in the reduction of yellow tetrazolium (MTT) to soluble, intensely purple formazan crystal in some potential cell lines. Formazan solution (10 mg/mL) is used to dissolve the yellow tetrazolium dye (50 mg) in the solution. It was filtered using 0.45-ptm Millipore filters and kept at 4C in the dark for 24 h after being vortexed violently for two minutes without homogenization. As MTT was light sensitive, the vial was covered in silver foil to keep it out of the light.

Viable lung and breast cancer cell lines can be counted using a hemocytometer or coulter counter after 24 h of incubation in 96 well plates in DMEM medium cultivated to the required density of 1 × 104 cells/mL. After that, MCF-7 cells were tested for drug treatment or control using the MTT assay, with samples containing varying doses of medicines (5 to 35 g/mL) administered to each well. On top of that, the treated cells (MCF-7) were kept for 24 h at 37 degrees Celsius in a humidified atmosphere with 5% CO_2. High-quality microplate readers measure the cell absorbance at 570 nm. Bioactive substances' IC50 (half maximum inhibitory concentration) values were established, and the optimal dosages were examined across a variety of time intervals. The IC50 values

were derived using dose-response curves in which a 50% decrease in inhibitory concentration relative to control cells was found.

Computational methods

All our theoretical calculations have been done using the Gaussian 09W package[16]. The Gaussian output files and molecular orbital reactions were imagined with Gauss-view 5 program[17]. B3LYP, CAM-B3LYP, B3PW91, PBEPBE and MPW1PW91 functional techniques have been used to conduct all of the high-level DFT calculations[18–21]. The molecular geometrical parameters has been performed on the vibrational modes at different function levels of theory and a variety of functions by assuming Cs symmetry point group. For the optimized structure, all fundamental vibration wavenumbers were computed using the five different functional methods.

The VEDA 4.0 program was used to determine the potential energy distributions of vibrational assignments of the estimated fundamental frequencies[22-28]. The GIAO technique has been used to calculate the chemical shifts in the DFT 1H and 13C NMR spectra. When it comes to determining the electronic transport characteristics of an object's electronic transport properties, the time-dependent DFT (TD-DFT) technique is used. The PBEPBE/6-311++G(d/p) theoretical level was also utilized to investigate FMOs and NLO properties. In order to satisfy the Lipinski Rule of 5 and calculate their drug likeness score, online Molinspiration Cheminformatics software was used to find the molecular characteristics of the prospective compounds[29]. Researchers used PBEPBE/6-311++G(d,p) to explore FMO features, as well as NLO features. The Lipinski Rule of 5, which is crucial for biological activity and also helps to calculate a title compound drug similarity score, was satisfied by the molecular characteristics, which were discovered using online molecular modelling software called Molinspiration Cheminformatics[29].

Result and Discussion

Molecular geometry

The 6-311++G(d,p) level of theory was used to compute the DMP3H molecule's ground state optimal structure (bond lengths, bond angles and dihedral angles). The PBEPBE has a worldwide minimum energy of –1259.55230009 a.u. There is no dipole moment in the molecular symmetrical (triangular planar) point group. Experimental values are contrasted with the optimized theoretical results. Figs. 1 depict the title compound's atom labeling and molecular packing diagrams. Results also show the selected geometrical properties such as bond lengths in and angles in degrees, that have been selected. To explain these inconsistencies, it is necessary to understand that quantum chemical calculation findings only apply to molecules in gaseous phase, whereas the observed results come from solid phase.

C–C bond distance in DMP3H is longer than the C3–C7 and C2–C11 single-bond lengths in heterocyclic ring, resulting in charge transfer in oxygen atoms in DMP3H. The actual optimized bond distance of C–O atoms in benzene ring is lower than 1.47Å, but a very important reduction observed in C13–C14, C14–C15 and C15–C16 distances of title compound is due to the attachment of methyl groups in 15 (3') and 14 (4') positions. These methyl and hydroxyl group substituents are important in biological activity. The computational distance value of C17–H18 is slightly shorter than the experimental value (0.92 Å) as a difference of (–0.31 Å) in PBEPBE level of theory.

Vibrational spectra

The DMP3H molecule belongs to Cs symmetric point group, which comprises 113 fundamental modes of vibration, in its optimum framed structure. This approach uses B3LYP, CAM-B3LYP, PBEPBE basis and an MPW1PW91 level of theory to assign harmonic vibrational wavenumbers. FT-IR and FT-Raman modes, as well as their PED assignments, (Supplementary material) together with the scaled harmonic frequencies. Based on normal coordinate analysis, the assignments for these basic vibrational bands have been determined by taking into account the spectral intensities of structure and the PED contributions from normal coordinate analysis with the same levels of theory.

The systematic overestimation of vibrational wavenumbers of DMP3H in the PBEPBE functional method is expected because of the presence of strong anharmonic contributions in a real chemical system, and therefore, the computed values of vibration are higher than the corresponding observed values. The disagreement between the theoretical calculations and experimental frequencies is rectified by the use of a

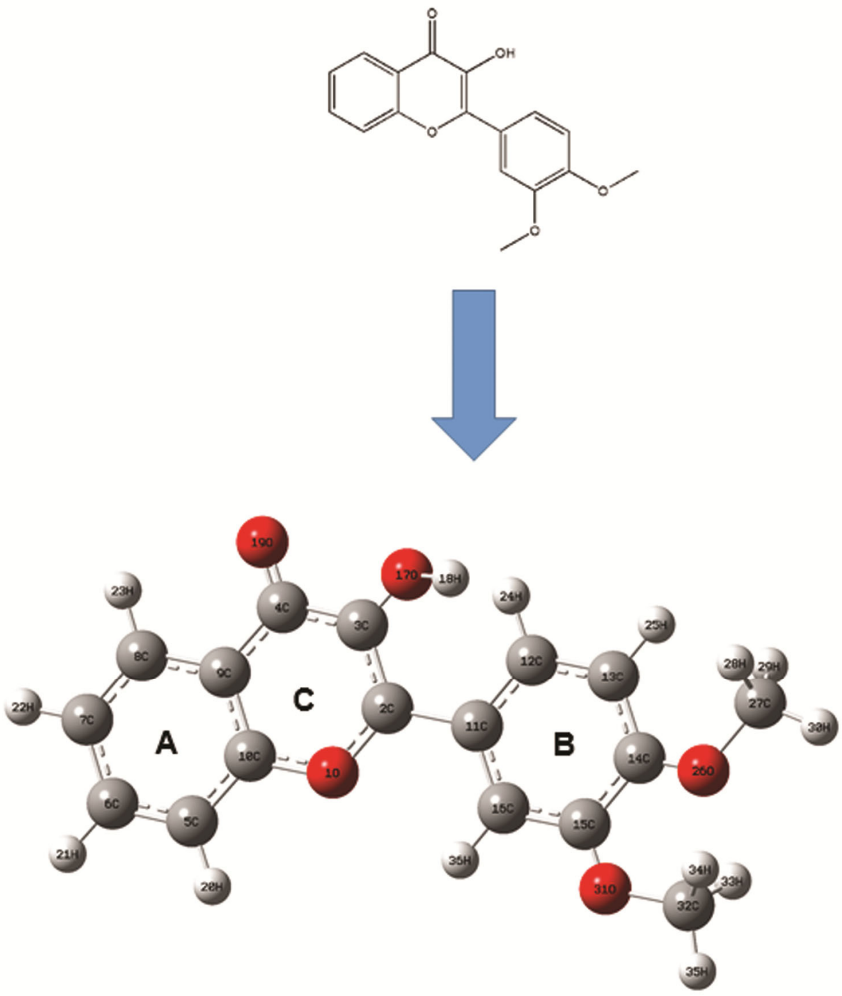

Fig. 1 — Optimized molecular structure of DMP3H.

scaling factor, and the calculated values show better conformity with the observed data. Figures 2 and 3 show the comparison between the experimental and simulated vibrational spectra of the title ligand. Our obtained results suggest that PBEPBE level theory could be a better DFT method to be used in calculated spectra. The bioactive molecule consists of aromatic benzene rings having two methoxy groups attached at B ring and a hydroxyl group at C ring, and hence a complete spectral analysis is discussed under four heads: (i) methyl (CH_3), (ii) methoxy (O-CH_3), (iii) hydroxyl (OH) and (iv) carbonyl group (C=O) vibrations.

Methyl group Vibrations

The title compound has four CH3 groups attached to the oxygen atom, and each of these groups can be associated to nine spectral bands[30–32]. It is possible to determine the motion of CH_3 groups by assigning different frequencies to each of the group's constituent atoms as well as different types of stretching and twisting (in-plane bending (ipb), out-of-plane bending (opb), and in-plane rocking/ out-of-plane rocking (ipr/opr)). Methyl group vibrations in heterocyclic aromatic compounds are often found in the 3000–2925 cm^{-1} range, which is an essential area for rapid identification. These high asym/sym stretching frequencies of 3390 and 3270 $cm^{-1}$are readily visible in FT-IR and FT-Raman spectra, which demonstrate the present molecule's 4' position methyl group substitution.

At 3399 and 3286 cm^{-1}, theoretically generated values are found to be more consistent with experimental frequencies. Due to the ipb and opb modes of CH_3, absorption wavenumbers in the range of 1490–1350 cm^{-1} are predicted. In FT-IR spectra,

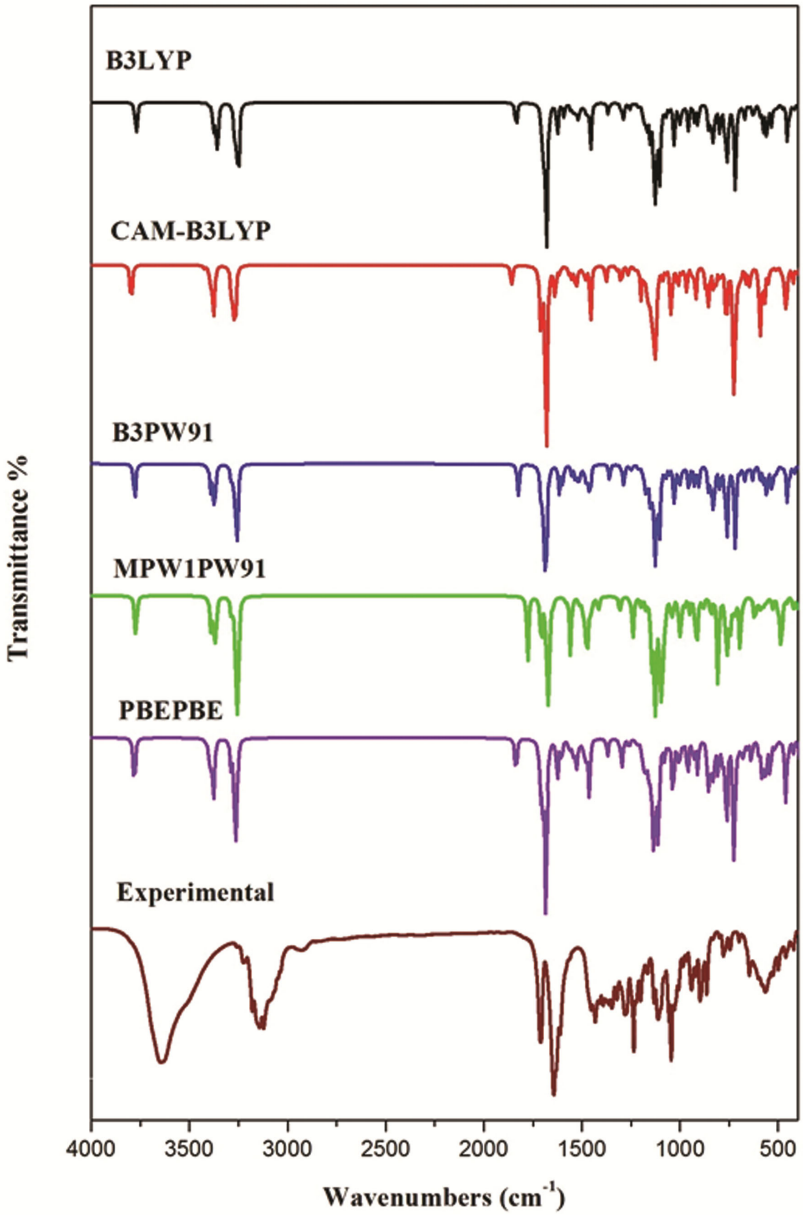

Fig. 2 — Experimental and simulated FT-IR spectra of DMP3H at various functional level theory.

the strong or medium bands detected at 1600, 1550 and 1517 cm^{-1}, as well as in FT-Raman spectra at 1603 and 1520 cm^{-1}, are thought to be generated by CH3 ipb vibrations, according to this theory. The opb vibrational frequencies were assigned to FT-IR and FT-Raman wavelengths of 1520, 1500 and 1512 cm^{-1}. Peaks in bending vibrations at 1599, 1541, 1522, 1519 and 1508 cm^{-1} were simulated using PBEPBE/6-311++G(d,p) level simulations with PED contributions ranging from 10% to 60%. Both spectra of the current compound exhibit medium intensity bands at 1448, 1210 and 1456, 1209 cm^{-1} for the CH3 group scissoring peaks. These frequencies are good correlated with the computed values, 1459 and 1206 cm^{-1} at PBEPBE method, respectively.

C–H vibrations

Heterocyclic structures have been shown to have C–H stretching[33, 34] frequencies between 3100 and 3000 cm^{-1}, which is consistent with C–H asym/sym stretching modes. The bands are observed at 3389, 3387, 3380, 3370 cm^{-1} and 3393, 3385, 3380, 3368 cm^{-1} in both spectra. The PBEPBE/6-311++G(d,p) scaling approach was used to calculated

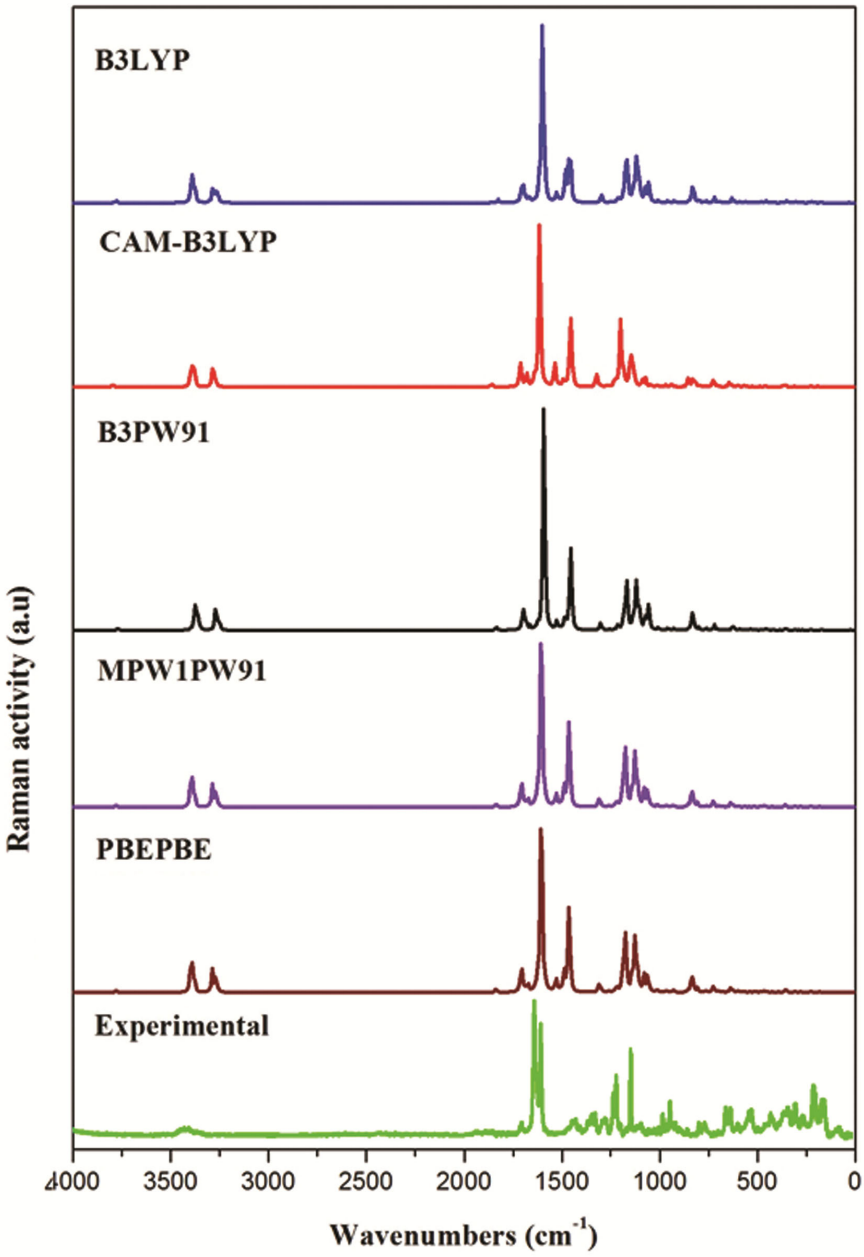

Fig. 3 — Experimental and simulated FT-Raman spectra of DMP3H at various functional level theory.

values of the following compounds: 3391, 3391, 3392, 3393, 3394 and 3395 cm^{-1}. According to experimental evidence, these values are in close agreement. Pure modes of 10–80 percent contributions appear in the PED corresponding to these vibrations. For the C–H ipb and opb absorption frequencies of polycyclic aromatic compounds[35] they mainly occurred in the spectrum areas of 1300 to 1000 and 950 to 800 cm^{-1}. These observed wavenumbers are 1293, 1250, 1185 and 1152 cm^{-1} in the FT-IR spectrum appear as medium to moderate and strong intensity bands. Results show the closely related bands of the C–H opb frequencies.

Hydroxyl group vibrations

The hydroxyl stretching spectral beak usually appears in the 3610–3640 cm^{-1} region[36]. Both spectra show O–H stretching wavenumbers of 3790 cm^{-1} and 3800 cm^{-1} in the present compound, with computed values of 3795 cm^{-1} with 99 percent PED contribution. Pure mode is a manifestation of this basic vibration mode. It is in this region that the O–H

ipb spectral intensities may be seen. Theoretically, a large and strong absorption band with a theoretical value of 1485 cm^{-1} with 69 percent PED in the FT-IR spectrum was found at 1482 cm^{-1} in FT-IR and 1483 cm^{-1} in FT-Raman spectra. The computed findings were quite near to the real results in terms of accuracy. These frequency are identified at 955 and 960 cm^{-1}, respectively, with a weak amplitude in the FT-IR/FT-Raman spectrum for the opb frequency band at 958 cm^{-1}.

C–O group vibrations

The title molecule contains a single bond carbonyl functional groups attached with 3, 3' and 4' positions of the benzene ring. The Three normal mode frequencies associated with the C–O group are sym/asym stretching, in/out plane bending, wagging, twisting, scissoring and rocking bands. Sym/asym stretching bands of C–O are often seen in the 1360–1300 cm^{-1} range[37]. Simply stating, in the FT-Raman spectrum, the asymmetric and symmetric C–O stretching vibration modes may be found at wavelength of 1300, 1221, 1210, 1190 and 1160 cm^{-1}, respectively. At 1303, 1215, 1206, 1191 and 1181 cm^{-1}, their calculated intensity peaks exactly match the real observations. In the FT-IR and FT-Raman spectra, the C–O group out-of-plane bending has frequencies of 1024, 950, 710 cm^{-1} and 1032, 952, 697 cm^{-1}. It is possible to get experimental intensities that match their theoretical equivalents by PED of 10 to 20% at 1030, 957 and 695 cm^{-1}. In addition, experimental evidence good agreement with calculated values.

C–C vibrations

The C–C and C=C stretching vibration frequencies of aromatic hydrocarbon rings are typically found in the 1650–1430 cm^{-1} range. In general[38,39], the vibrational modes are given 1625–1590 cm^{-1}, 1590–1575 cm^{-1}, 1540–1470 cm^{-1} and 1465–1430 cm^{-1}. The FT-IR spectra in the current study have detected significant aromatic C–C stretching vibrations at 1572, 1624, 1522 and 1482 cm^{-1}. Stretching modes at 1620, 1570, 1532, 1525 and 1483 cm^{-1} were found in the FT-Raman spectrum. The spectral intensities are all in the anticipated range when compared to the wavenumbers predicted by the theoretical model.

FT-IR and FT-Raman spectroscopy show the C–C ipb vibrations at 1012 and 950 cm^{-1}, while the bending modes at 1004, 952 and 843 cm^{-1} are revealed by FT-IR and FT-Raman spectroscopy, respectively. This means that the calculated aromatic stretching vibration at 1556 cm^{-1} is closer to the observed peak at 1552 and 1550 cm^{-1}. C–C opb vibration may be detected at 600, 582 cm^{-1} and 615, 580 cm^{-1} in the FT-IR and FT-Raman spectra of this molecule. Theoretically expected values of 615 and 574 cm^{-1}, according to theoretical predictions and experimental data of PBEPBE/6-311++G(d,p) simulations are in good agreement.

HOMO-LUMO

Physics and Chemistry use the molecular orbital (MO) hypothesis and its characteristics the most. The most reactive location in large conjugated electron systems, which play an important role in optical and biological activity, may be predicted using electron densities[40]. A chemical structure's electron donating and receiving abilities may be determined using the frontier molecular orbital (HOMO-LUMO) energies contained in its structure. A measure of intramolecular charge transfer, the border orbital energy level is also particularly important in chemical compound stability and reactivity[41]. (ICT). Chemical stability and low reactivity are usually linked to molecules with a small HOMO-LUMO energy gap. The HOMO-LUMO electron density map and associated energy values have been determined and shows that the HOMO orbital of the compound's - nature is mostly placed over the carbonyl group and somewhat over the oxygen group in its structure, while the bioactive compound's empty LUMO orbital is positioned over the aromatic benzene rings. The value of the energy gap between the HOMO and LUMO is –2.47 eV. Bioactivity of DMP3H was improved by the conjugation of electron-donating groups and electron-accepting groups, according to the study findings.

Organic and inorganic molecules without metals are less able to conduct electricity as a result of the HOMO-LUMO energy mismatch. Reactivity in chemical processes can be measured using the following terms: chemical potential (μ), chemical hardness (η), global softness (S), the electrophilicity index (ω) and electronegativity (χ). Table S3 (Supplementary material) presents the results of calculating chemical hardness and softness, as well as local descriptors, using the frontier orbital energy values and chemical hardness than the PBEPBE technique. Descriptors including chemical hardness (η), global softness (S), electron affinity (EA), and ionization potential (IP) have been derived from quantum chemistry calculations. The HSAB (Hard-

Soft Acid-Base) theory fundamentally measures the resistance to deformation or change of the ions radius, atoms under small perturbations of the charge cloud during physical and chemical reactivity. The greater the E_{HOMO}–E_{LUMO} energy gap, the more probable it is that the molecule has a hard acid or base and a low value. The E_{HOMO}–E_{LUMO} energy gap indicates a molecule with a soft acid and base.

NLO analysis

Title molecule's electric dipole moment, polarizability (α), and first-order hyper-polarizability (βtot) are anticipated to be comparable to urea using the DFT technique with various function levels of theory[42]. The first order α_{tot} and β_{tot} is the most significant parameter of the nonlinear optical behavior of the molecule. Furthermore, the dipole polarizability has a direct relation between the ligand binding energies; a highly polarizable mediated ligand is possible to binding more potential interaction to its target protein structure as compared to a weakly polarizable ligand. The mean high polarizability and hyperpolarizability at DFT/PBEPBE/6-311++G(d,p) are computed to be 13.855×10^{-24} e.s.u. and 2.8502×10^{-30} e.s.u is presented in Table S4 (Supplementary material), respectively. The high value of hyperpolarizability estimation of novel drug compound could be improving its pharmacological or biological activity. The title compound, determined hyperpolarizability is compared to the standard urea level (0.13×10^{-30}esu)[43]. The DMP3H compound has a dipole moment calculated at 2.6860 Debye in the PBEPBE, which is slightly higher than 2.3877 Debye in B3LYP, 2.2289 Debye in CAM-B3LYP, and 2.3874 Debye in B3PW91 and 2.3860 Debye in MPW1PW91, respectively.

Hirshfeld surface analysis

Researchers used Hirshfeld surface analysis and 2D fingerprint plots to better understand the molecular H-bond interactions in crystal structure. Hirshfeld surface color-coded maps by d_{norm} highlights the pinpoint intermolecular natural shorter and longer intermolecular contacts in the crystal structure[44,45]. The red color spots represent the strong (large) and weak (small) intermolecular interactions of the molecule. On the Hirshfeld surface, detailed information about d_{norm} is presented to illustrate the intermolecular interactions (de and di), shape-index and curvedness of the crystal structure in Fig. 4. Hirshfeld surface analysis and 2D fingerprint plots were used to examine the molecular H-bond interaction in crystal structure in Fig. 5. The important non-covalent interaction of 63.1% from H···H contacts, which are exposed as bifurcated long spikes in the fingerprint plots. The second hydrogen bond contributions to the surface contacts are from H···O (18.3%) interaction due to the occurrence of four oxygen atoms in the molecule. The strong repulsion steric effect is characterized via the blue color spikes in the regions. Furthermore, other bonding interactions contribution is observed for and H···C (18.7%) contacts, which can be attributed to π–π stacking behavior.

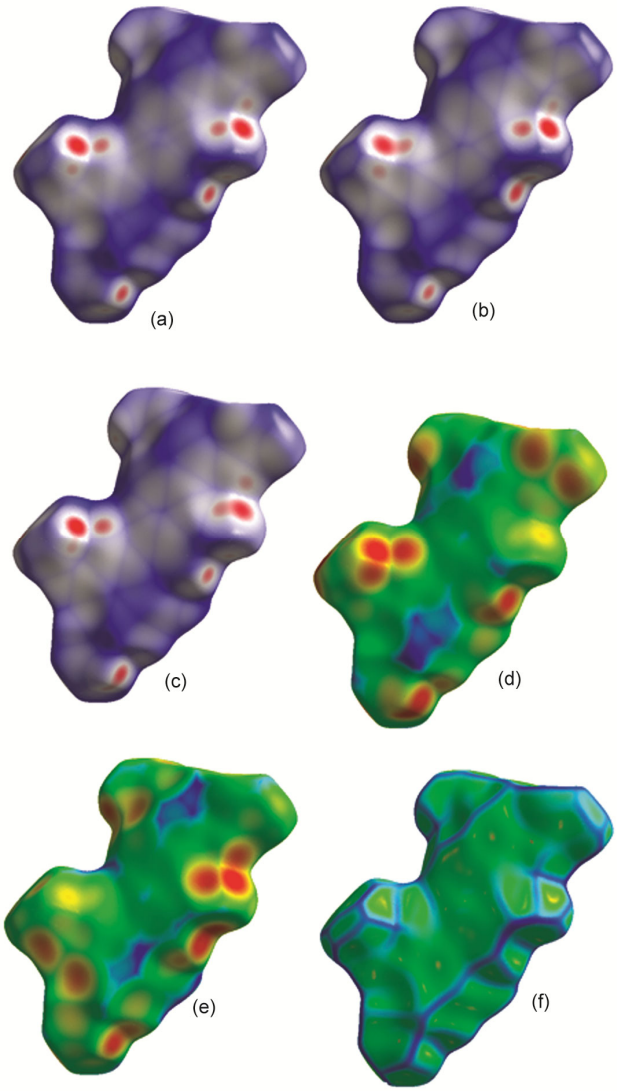

Fig. 4 — The Hirshfeld surface of crystal mapped with (a) di, (b) de, (c) d norm (e), (d) d norm (i), (e) d norm and (f) shape-index of the title compound.

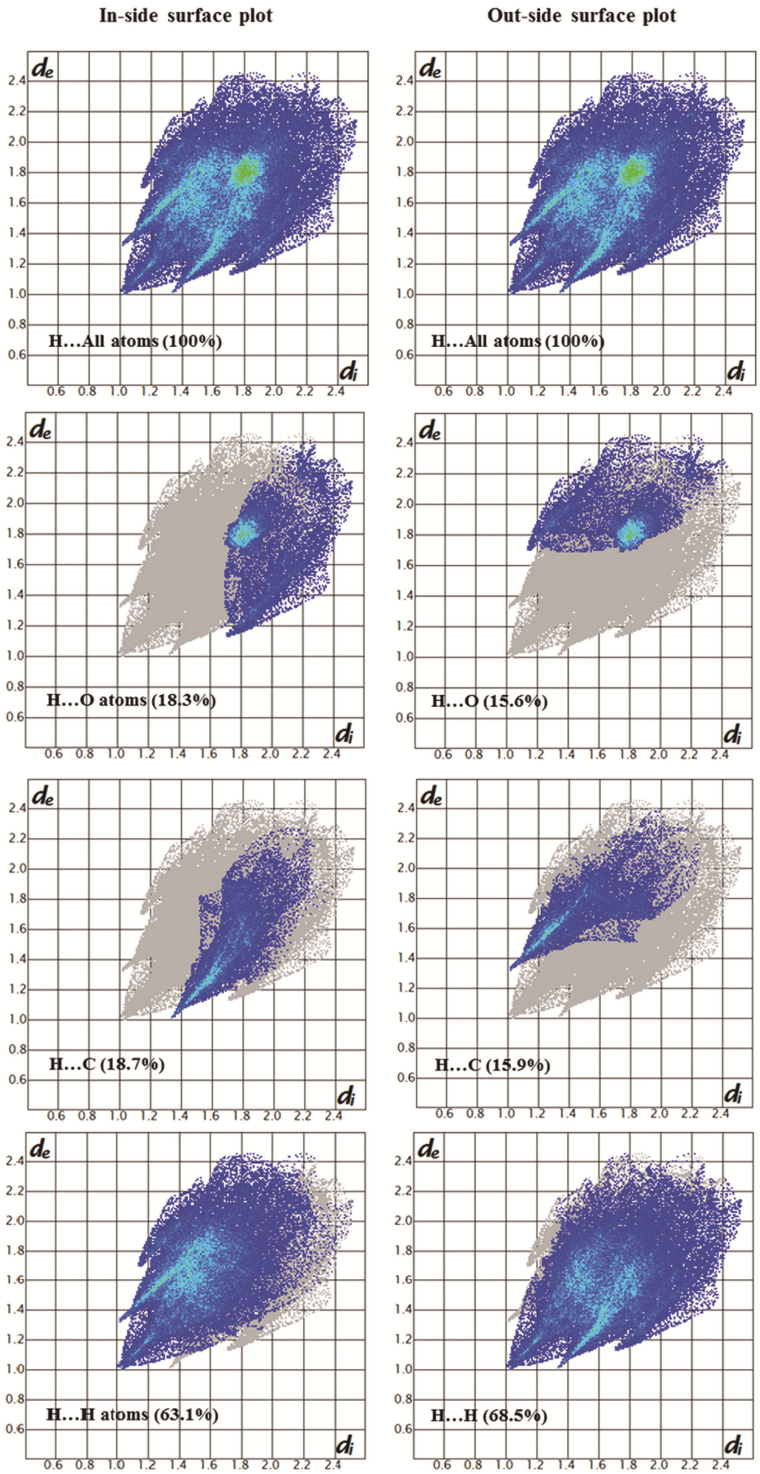

Fig. 5 — 2D fingerprint plots of the title molecule and the contribution rates to the whole intermolecular interactions are shown.

NMR spectra

The PBEPBE/6-311++G(d,p) basis set and the gauge independent atomic orbital (GIAO) technique were used to forecast the DMP3H ^{1}H and ^{13}C NMR chemical signals. NMR spectra in Fig. 6 illustrate theoretical and actual isotropic NMR spectra (a and b). The aromatic hydrocarbon rings provide shifts in overlapped regions of the 13C spectrum with signal

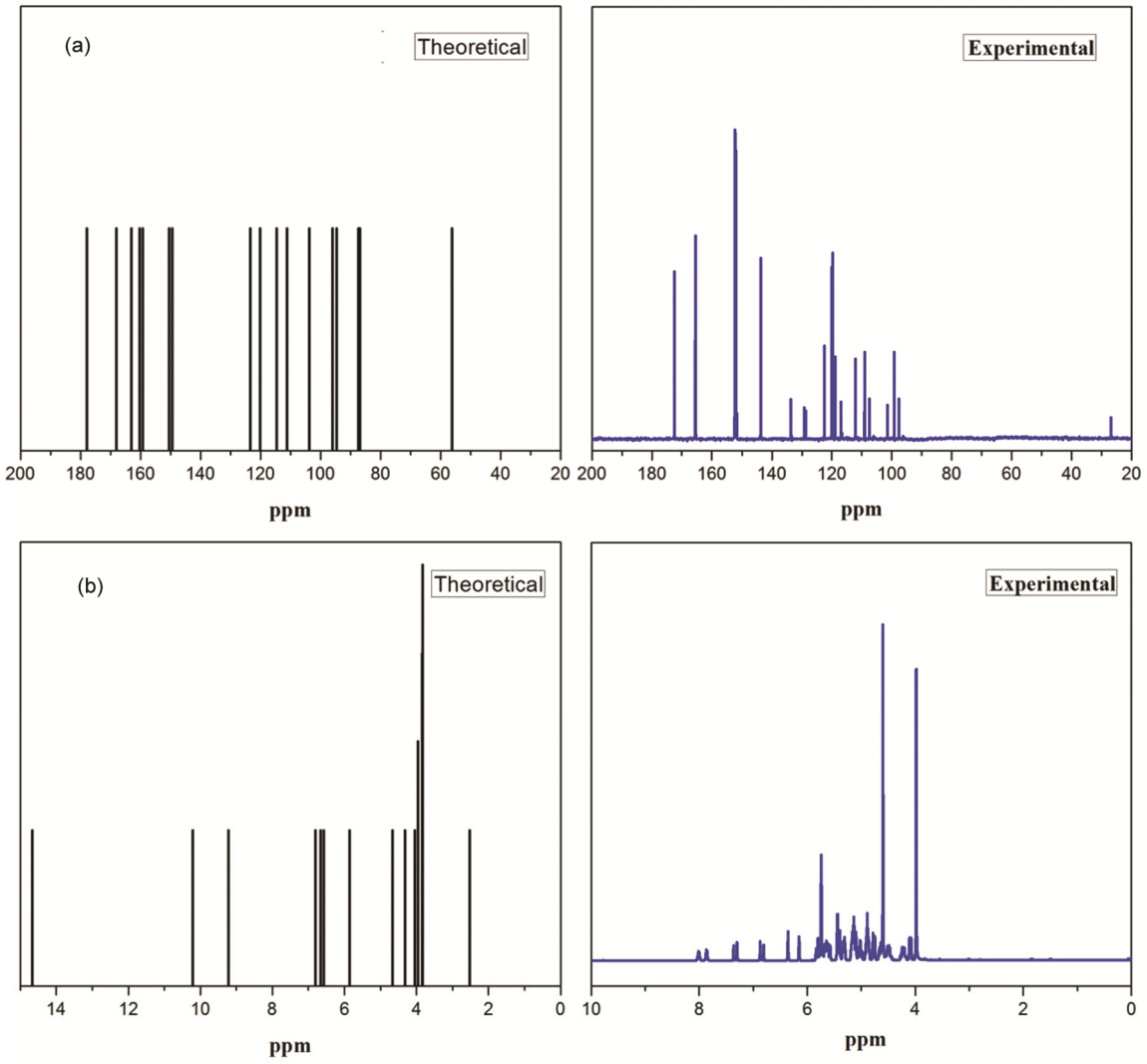

Fig. 6 (a) — Simulated and experimental ^{13}C NMR spectra of DMP3H; (b) Simulated and experimental ^{1}H NMR spectra of DMP3H.

peaks were observed to be 164.8–99.4 ppm and found to be 178.3–95.1 ppm range by DFT level. In the present study, the chemical signals of oxygenated C3 (O17) and C4 (O19) atoms are high, compared to other ring carbon atoms. All of the carbon-theoretical figures correspond well with that seen in the field. C7 and C8 had measured ^{13}C NMR chemical signal levels of 160.1 and 159.3 ppm, compared to theoretical values of 168.2 and 169.3 ppm. Chemical changes in heterocyclic rings are set down field on the other hand. Signals at 100.4, 156.0, 99.4, 140.6 and 155.3 ppm are found for C2, C5, C6, C9 and C10, respectively. Table 1 shows the predicted and experimental isotropic chemical shifts (with respect to TMS) that can be observed.

To compare the experimental and computational results, DFT theory was used to calculate the proton (1H) isotropic chemical shift of TMS values. It was found that it ranged from 10.3–4.0 ppm. Since the chemical shifts of flavone ring of the title compound were theoretically given seven proton signals, which is calculated at 5.9, 6.7, 6.6, 6.7, 10.3, 3.9 and 4.3 ppm. The experimental values were observed at 5.4, 7.1, 7.3, 6.1, 9.8, 4.7 and 4.5 ppm. For PBEPBE/6-311++G(d,p) level theory, the highest values for proton of NMR signals from the H24 atom exhibit an upfield shift of 9.8 (exp.) and 10.3 (cal.) ppm, whereas the simulated peak value is seen at 4.6 ppm (exp.) and 3.8 ppm (cal.) of H33. There were also additional proton signals for aromatic hydrogen atoms such as H28 at 4.7 ppm whereas the predicted values are at 4.8 (H29), 4.8 (H30), 4.6 (H33), 4.7 (H34) and 4.8 (H35). Using the NMR signal value, it may be learned about the proton's chemical environment (e.g.,

Table 1 — The theoretical and experimental isotropic ^{13}C and ^{1}H chemical signals in DMSO as a solvent using PBEPBE/6-311++G(d,p) level of theory of DMP3H.

Atoms	Chemical Shift (ppm)				
	Exp.	PBEPBE	Atoms	Exp.	PBEPBE
C_2	100.4	95.1	H_{18}	5.7	6.0
C_3	164.8	162.9	H_{20}	5.4	5.9
C_4	162.3	103.6	H_{21}	7.1	6.7
C_5	156.0	159.3	H_{22}	7.3	6.6
C_6	99.4	96.1	H_{23}	6.1	6.7
C_7	160.1	168.2	H_{24}	9.8	10.3
C_8	159.3	169.3	H_{25}	4.7	3.9
C_9	140.6	136.6	H_{28}	4.7	3.9
C_{10}	155.3	160.0	H_{29}	4.8	4.0
C_{11}	120.5	123.7	H_{30}	4.8	4.1
C_{12}	115.4	111.6	H_{33}	4.6	3.8
C_{13}	144.4	149.7	H_{34}	4.7	4.1
C_{14}	148.0	149.0	H_{35}	4.8	4.2
C_{15}	115.8	115.2	H_{36}	4.5	4.3
C_{16}	121.3	119.7			
C_{27}	121.6	120.3			
C_{32}	121.7	120.8			

Table 2 — Biological property/phytochemical activity parameters of title compound.

Parameters	**Values**
miLogP	3.11
TPSA	87.38
natoms	26
MW	358.35
nON	7
nOHNH	1
Volume	310.20
nrotb	5
GPCR	–0.12
Kinase inhibitor	0.17
Nuclear receptor ligand	0.19
Drug like score	0.92
Ion channel modulator	–0.27
Protease inhibitor	–0.24
Enzyme inhibitor	0.12
Hydrogen bond donor	2
Hydrogen bond acceptor	5

aliphatic, aromatic or aldehydic), and the proton in the ortho and para locations is protected from electron-withdrawing effects while the proton in the deshielded position is shielded from electron-donating methyl groups.

Drugs scans approach

The drugs scans approach have been performed to calculate whether or not the designed inhibitors fulfil the drug-likeness conditions. The bioactive molecule's drug similarity and ADMET characteristics were assessed using Lipinski's rule of five (Ro5)[46,47]. A molecular weight (MW) of less than 500, a partition coefficient logP of less than 5, a topological polar surface area (TPSA), and less than five H-bond donors (HBD) and H-bond acceptors (HBA) are among properties. These results were verified using Molinspiration software[47]. The title compound exhibit good bioactivity score and drug-like physicochemical parameters are given in Table 2. However in this case, the peaks of the HBA and HBD were computed to be 5 acceptors and 2 donors respectively. Hence, the LogP and TPSA have been measured to be 3.11 and 87.38 A^2. These values of corresponding rule of five are obeyed; dissolution rate of the drug, solubility and permeability in drug discovery of the ligand was determined to be good and has certain pharmacological activity. Moreover, the GPCR, modulation of ion channel function, modulation of nuclear receptor activities (NCR) and the particular inhibitors are calculated to be –0.12, –0.19 and –0.24, it was established to controls several important diseases. This medication has a high bioactivity score and is a promising inhibitor in the treatment of breast cancer, as indicated by Lipinski's rule results.

Molecular docking analysis

Computer-aided medication design and development for the treatment of many illnesses has become increasingly dependent on the docking technique. Computer simulations provide plausible ligand-receptor complex binding interactions that may be used to verify the experimental results. Molecular docking study of DMP3H drug against 1AO6 and 4HJO structures was performed by using the open source AutoDock 4.2 and AutoDock Vina tools program package[48,49]. The 3D model of 1AO6 and 4HJO protepins was downloaded from Structural Bioinformatics Protein Data Bank (RCBS-PDB)[50, 51]. Using PyMolsoftware and the Lamarckian genetic algorithm (LGA), the AutoDock tools determined the optimal binding affinity for ligand receptor binding engagements.

The aim of this present investigation is to examine the drug affinity and activity of DMP3H (O-CH_3, OH and O groups) with the binding site of target proteins by the AutoDock suite of program. The visual representation of possible binding sites and amino acid residues interacting of title compound with target proteins (1AO6 and 4HJO) are shown in Fig. 7 (a and b). This systematic analysis of DMP3H displayed that the entire was focused in the active sites of groove of the protein enzymes. Table 3 shows the binding free

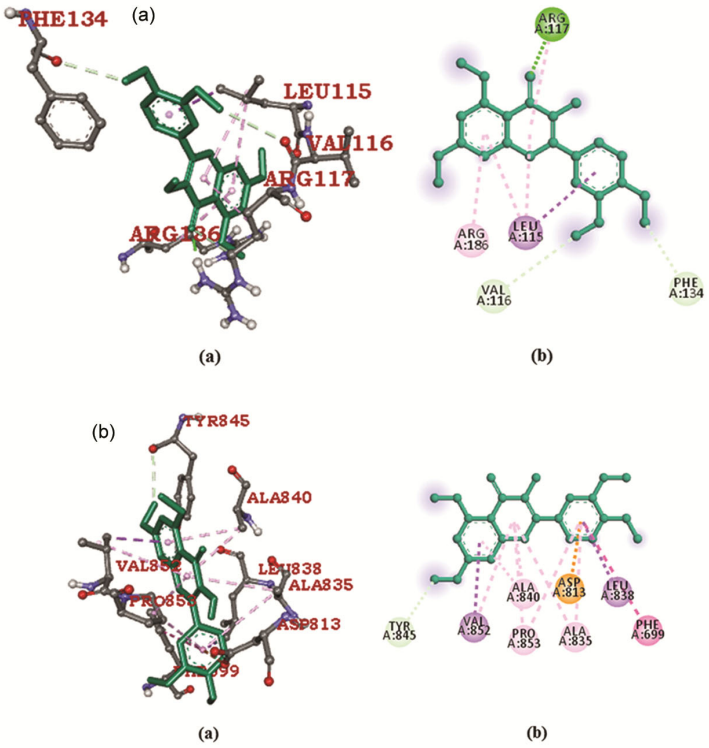

Fig. 7 — (a) 3D docking poses(a) and 2D representation of polar and non-polar residues (1AO6) (b) and (b) 3D docking poses(a) and 2D representation of polar and non-polar residues (4HJO) (b).

Table 3 — The docking, Bond distance, score and H-bond interaction of DMP3H ligand.

Ligand Target	protein	Binding affinity	Binding residue	Type	Atoms	Interactions
DMP3H	1AO6	–8.6	ARG:A 117	Arginine	O18	Conventional
			ARG:A 186	Arginine	A ring	Pi-Alkyl
			LEU:A 115	Leucine	B ring	Pi-Sigma
			VAL:A 116	Valine Phenylalanine	H35	Pi-H-Donor
			PHE:A 134		H36	Pi-H-Donor
	4HJO	–7.5	TYR:A 845	Tyrosine Valine	H39	Pi-H-Donor Pi-Sigma
			VAL:A 852	Alanine	A ring	Pi-Alkyl
			ALA:A 840	Proline	C ring	Pi-Alkyl
			PRO:A 853	Aspartic acid Alanine	C ring	Pi-Sulfur
			ASP:A 813	Leucine	B ring	Pi-Alkyl
			ALA:A 835	Phenylalanine	B ring	Pi-Sigma
			LEU:A 838		B ring	Unfavorable
			PHE:A 699		B ring	

energy, atom hydrophobic interactions, and the distance between the donor and acceptor atoms. According to the docking results of the DMP3H ligand is oriented with the binding residues of protein 1AO6 forming five H-bond interactions with ARG A:117, ARG A:186, LEU A:115, VAL A:116 and PHE A:134. Also, it has the better hydrogen-binding interaction (–7.5 kcal/mol) with the 1AO6 protein, resulting in high inhibition potency. This high inhibition energy suggests a more favorable binding mode. The centre of A aryl ring exhibited hydrophobic Pi-Alkyl and Pi-Sigma interactions with ARG A:186 and LEU A:115 having 5.62 and 4.06 distances.

The ligand is immensely bonded with the enzyme active site of amino acid residues VAL A:116 and PHE A:134 by bi donor hydrogen bond and hydrophobic interactions conduct to more antiviral

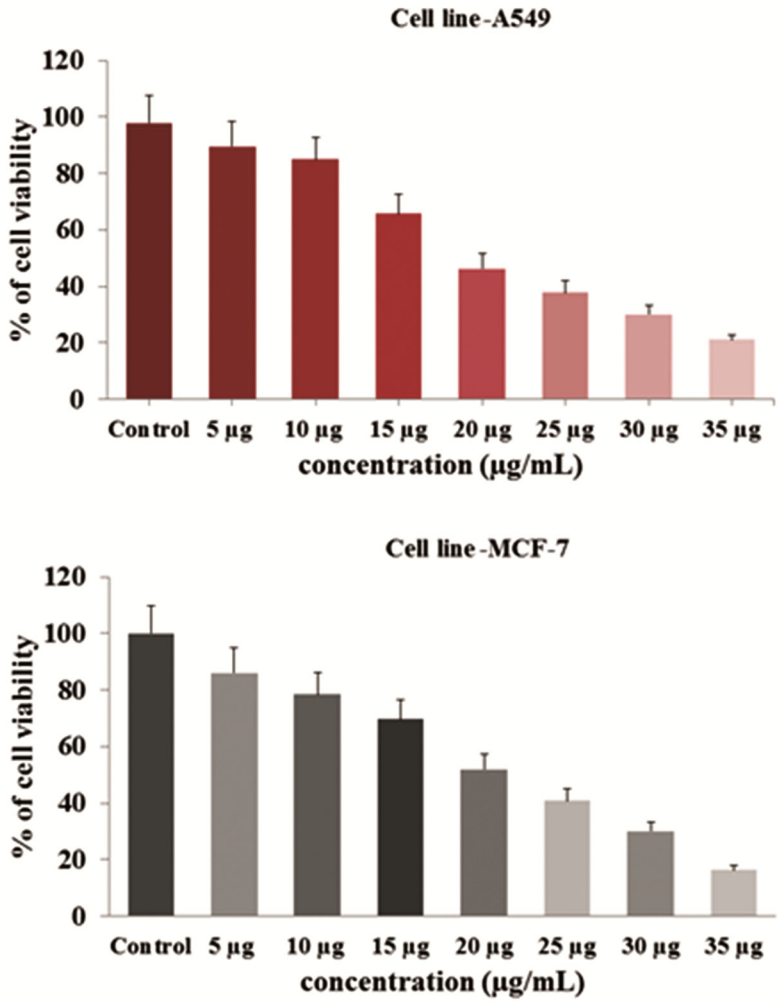

Fig. 8 — Effect of the extracts on cell viability and proliferation.

activity. For PDB ID: 4HJO protein structure, the amino acid residues ASP A:813, ALA A:835, LEU A:838 and PHE A:699 were involved in sigma, sulfur and sigma interaction with the centre of B aromatic ring with 4.29, 5.10, 3.28 and 5.62 Å bond length, respectively. The binding free energy (ΔGb) of 4HJO protein is found to be –8.6 kcal/mol. In addition, the A and C aromatic rings with a pi-Sigmal and pi-Alkyl interactions was surrounded by the hydrophobic residues including VAL A:852, ALA A:840, PRO A:853 and ALA A:835 had been formed with bond distances 4.15, 3.70, 4.15 and 5.10 Å. It was found that the H34-TYR845 pi-donor H-bond had a length of 4.12 nm. The molecular docking results and the formation of strong interaction of H-bonding interactions proposed that the mentioned ligand performs to be a promising anticancer agent.

MTT assay

The MTT assay is used to measure cellular metabolic activity as an indicator of cell viability, proliferation and cytotoxicity. The cytotoxic activity of DMP3H was estimated in two different cell lines as percent cell viability at concentration-dependent manner of the compound. Anti-proliferative activity was found in human lung and breast cancer cell lines when these compounds were tested. As shown in Fig. 8, the cell proliferation or cell cytoxicity measured using the MTT assay in both cell lines significantly decreased with different concentrations of DMP3H when compared to untreated cells and control cells.

According to the title compound exhibited cytotoxicity at 30–35 µM/mL and least at 30 µM/mL concentration in both A549 and MCF-7 cell lines. The IC_{50} value signifies the inhibition concentration of the

drug required to kill 50% of the cells. That is antiproliferative activity of title drug against A549 and breast MCF-7 human cancer cell lines exhibited IC_{50} values of 22.3 Mm and 18.4 Mm. These results propose that DMP3H compound could serve as a promising agent for further cancer treatment.

Conclusion

In the present investigation, the spectroscopic and molecular profiles of the molecule DMP3H have been recorded. PBEPBE/6-311++G (d,p) was utilized as a functional approach to investigate the molecule's structural, vibrational and NLO properties. The PBEPBE approach, which has greater agreement with experimental data, is used to estimate the optimal geometric parameters, vibration spectrum peak and NMR chemical shifts (1H and 13C). The lower value of HOMO-LUMO energies shows biological activity, high kinetic stability and low chemical reactivity. The high polarizability value of the compound DMP3H possesses considerable improvement in its bioactivity. In addition, the results of molecular docking on cancer-active 1AO6 and 4HJO proteins demonstrate that hydrogen bond interactions with adjacent residues had free energies of –7.5 and –8.6 kcal/mol, respectively. The cytotoxicity of DMP3H against A549 and MCF-7 cell lines was studied using the MTT cell viability test to determine its anticancer activity. Our findings provide a promising foundation for the novel design of flavone medicines and will be useful in the antiviral drug development of DMP3H pharmacological and biochemical effects for cancer treatment.

References

1 Sung H, Ferlay J, Siegel R L, Laversanne M, Soerjomataram I, Jemal A & Bray F, *CA Cancer J Clin*, 71 (2021) 209.
2 Siegel R L, Miller K D, Fuchs H E & Jemal A, *CA Cancer J Clin*, 71 (2021) 7.
3 Pucci C, Martinelli C & Ciofani G, *Ecancermed Sci*, 13 (2019) 961.
4 Dasari S & Tchounwou P B, *Eur J Pharmacol*, 740 (2014) 364.
5 Wang X, Zhang H & Chen X, *Cancer Drug Resist*, 2 (2019) 141.
6 Ekalu A & Habila J D, *Beni-Suef Univ J Basic Appl Sci*, 9 (2020) 1.
7 Pandey K B & Rizvi S I, *Oxid Med Cell*, 2 (2009) 270.
8 Beckman C H, *Physiol Mol Plant Pathol*, 57 (2000) 101.
9 Block G, Patterson B & Subar A, *Nutr Cancer*, 18 (1992) 1.
10 Scalbert A, Johnson I T & Saltmarsh M, *Am J Clin Nutr*, 81 (2005) 215.
11 Singh M, Kaur M & Silakari O, *Eur J Med Chem*, 84 (2014) 206,
12 Middleton E, Kandaswami C & Theoharides T C, *Pharmacol Rev*, 52 (2000) 673.
13 Havsteen B H, *Pharmacol Ther*, 96 (2002) 67.
14 Masraksa W, Tanasawet S, Hutamekalin P, Wongtawatchai T & Sukketsiri W, *Nutr Res Pract*, 14 (2020) 127.
15 Mosmann T, *J Immunol Methods*, 65 (1983) 55.
16 Frisch M J, Trucks G W, Schlegel H B, Scuseria G E, Robb M A, Cheeseman J R, Scalmani G, Barone V, Petersson G A, Nakatsuji H, Li X, Caricato M, Marenich A, Bloino J, Janesko B G, Gomperts R, Mennucci B, Hratchian H P, Ortiz J V, Izmaylov A F, Sonnenberg J L, Williams-Young D, Ding F, Lipparini F, Egidi F, Goings J, Peng B, Petrone A, Henderson T, Ranasinghe D, Zakrzewski V G, Gao J, Rega N, Zheng G, Liang W, Hada M, Ehara M, Toyota K, Fukuda R, Hasegawa J, Ishida M, Nakajima T, Honda Y, Kitao O, Nakai H, Vreven T, Throssell K, Montgomery Jr J A, Peralta J E, Ogliaro F, Bearpark M, Heyd J J, Brothers E, Kudin K N, Staroverov V N, Keith T, Kobayashi R, Normand J, Raghavachari K, Rendell A, Burant J C, Iyengar S S, Tomasi J, Cossi M, Millam J M, Klene M, Adamo C, Cammi R, Ochterski J W, Martin R L, Morokuma Farkas K O, Foresman J B & Fox D J, Gaussian 09W Program Gaussian, Inc., Wallingford CT, (2016).
17 Dennington R, Keith T & Millam A J, *Gauss View, Version 6*, Semichem Inc., Shawnee Mission, KS, (2016).
18 Becke A D, *J Chem Phys*, 109 (1998) 2092.
19 Lee C, Yang W & Parr R G, *Phys Rev B*, 37 (1988) 785,
20 Govindarajan M, Ganasan K, Periandy S & Mohan S, *Spectrochim Acta Part A*, 76 (2010) 12.
21 Jamróz M H, *Spectrochim Acta Part A*, 114 (2013) 220.
22 Pulay P, Fogarasi G, Pongor G, Boggs J E & Vargha A, *J Am Chem Soc*, 105 (1983) 7037.
23 Rauhut G & Pulay P, *J Phys Chem A*, 99 (1995) 3093.
24 Mtat D, Touati R, Guerfel T, Walha K & Hassine B B, *Crystallogr Rep*, 61 (2016) 1064.
25 Runge E & Gross E K, *Phys Rev Lett*, 52 (1984) 997.
26 Kohn W, Becke A D & Parr R G, *J Phys Chem A*, 100 (1996) 12974.
27 Parr R G & Pearson R G, *J Am Chem Soc*, 105 (1983) 7512.
28 Politzer P & Abu-Awwad F, *Theor Chem Acc*, 99 (1998) 83.
29 Zhai X J, Cheng H R, Long H L, Mao W K, Cao L, Xiao B R & Li R Q, *Genet Mol Res*, 14 (2015) 5399.
30 Kalsi P S, Spectroscopy of Organic Compounds, sixth ed., New Age International (P) Limited Publishers: New Delhi, (2005).
31 Adant C, Dupuis M & Bredas J L, *Int J Quantum Chem*, 56 (1995) 497.
32 Parimala K & Manimegalai S, *Mater Today Proc*, 60 (2022) 1575.
33 Buyukuslu H, Akdogan M, Yildirim G & Parlak C, *Spectrochim Acta A*, 75 (2010) 1362.
34 Socrates G, Infrared and Raman characteristic group frequencies: tables and charts, John Wiley & Sons, (2004).
35 Parimala K & Manimegalai S, *MaterToday Proc*, 59 (2022) 636.
36 Gladis A E, Joseph V S & K Parimala, *Spectrochim Acta Part A*, 136 (2015) 1557.
37. Palafox M A, Rastogi V K, Mittal L, Kiefer W & Mital H P, *Int J Quantum Chem*, 106 (2006) 1885.
38 Parimala K & Manimegalai S, *Indian J Pure Appl Phys*, 60 (2022) 662.

39 Varsányi G, Assignments for vibrational spectra of seven hundred benzene derivatives John Wiley & Sons: New York, 1 (1974).
40 Ramachandran G, Muthu S & Renuga S, *Spectrochim Acta Part A*, 107 (2013) 386.
41 Aihara J I, *J Phys Chem A*, 103 (1999) 7487.
42 Parimala K & Manimegalai S, *Indian J Pure Appl Phys*, 60 (2022) 49.
43 Tanaka H & Toy M, *J Mol Struct*, 1068 (2014) 189.
44 Sheena Mary Y, Shyma Mary Y, Rad A S, Yadav R, Celik I & Sarala S, *J Mol Liq*, 330 (2021) 115652.
45 McKinnon J J, Spackman M A & Mitchell A S, *Acta Crystallogr Sect B*, 60 (2004) 627.
46 Costa R A, Pitt P O, Pinheiro M L B, Oliveira K M T, Salome K S, Barison A & Costa E V, *Spectrochim Acta Part A*, 174 (2017) 94.
47 Lipinski C A, Lombardo F, Dominy B W & Feeney P J, *Adv Drug Deliv Rev*, 46 (2001) 3.
48 Huey R, Morris G M, Olson A J & Goodsell D S, *J Comput Chem*, 28 (2007) 1145.
49 Shafique M, Garg M L & Nandel F S, *Biophys Chem*, 6 (2015) 54.
50 Madej T, Lanczycki C J, Zhang D, Thiessen P A, Geer R C, Marchler-Bauer A & Bryant S H, *Nucleic Acids Res*, 42 (2014) D297.
51 Park J H, Liu Y, Lemmon M A & Radhakrishnan R, *Biochem J*, 448 (2012) 417.